High-Fidelity CFD Verification Workshop 2024: Shock-Dominated Flows

Kevin Holst [*]
University of Tennessee, Knoxville, TN 37996, U.S.A.

Chongam Kim [†]
Seoul National University, Seoul 151-742, Republic of Korea

Matthew J. Zahr [‡]
University of Notre Dame, Notre Dame, IN 46556-5637, U.S.A.

I. Introduction

The first High-Fidelity CFD Verification Workshop will be held in 2024. While its scope has been expanded relative to its predecessors [1] that focused on high-order CFD methods, its mission is closely aligned with previous workshops: 1) provide an open and impartial forum for evaluating the status of CFD methods in solving a wide range of flow problems; 2) assess the performance of CFD methods through comparison to production CFD codes widely used in the aerospace industry with well-defined metrics; 3) support new research in CFD method development by providing validation cases and aid during development and improvement of codes; and 4) establish best practices for large-scale simulations. The test suite presented in this manuscript is focused on shock-dominated flows. The individual test problems have been chosen to reduce the barrier to participation, while still incorporating relevant supersonic and hypersonic flows.

II. Steady, inviscid, transonic flow: Gaussian bump in a channel

The first test problem is steady, inviscid, transonic flow over a smooth bump; a subsonic version of this problem was used as a verification case at the 5th International Workshop on High-Order CFD Methods and earlier workshops [1]. The goal of this problem is to assess the ability of CFD methods to preserve consistency and accuracy in the presence of an attached curved shock. It is also a relatively simple problem with low barrier to participation.

A. Geometry

The geometry of the domain is shown in Figure 1, and the bottom of the channel is located at
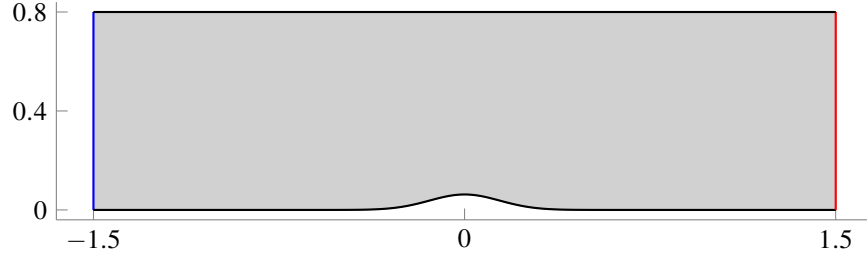
$$y(x) = 0.0625e^{-25x^2}. \tag{1}$$

B. Governing equations

The governing equations are the 2D Euler equations with a constant ratio of specific heats $\gamma = 1.4$. The freestream Mach number is $M_\infty = 0.7$. The top and bottom of the channel are both inviscid walls. The left boundary condition is specified as a subsonic inflow condition corresponding to a freestream temperature $T_\infty = 1$ and pressure $p_\infty = 1/\gamma$. The right boundary condition is specified as a subsonic outflow condition with back pressure $p = p_\infty$. The stagnation enthalpy remains constant throughout the domain with the value given by $H_\infty = 2.745$.

---

[*]Assistant Research Professor, Department of Electrical Engineering and Computer Science, University of Tennessee, Knoxville, TN, 37996. Email: kholst@utk.edu. Senior AIAA member.

[†]Professor, Department of Aerospace Engineering, Institute of Advanced Aerospace Technology, 1 Gwanak-ro, Gwanak-gu; chongam@snu.ac.kr. AIAA Associate Fellow.

[‡]Assistant Professor, Department of Aerospace and Mechanical Engineering, University of Notre Dame, Notre Dame, IN, 46556-5637. Email: mzahr@nd.edu. AIAA member.

Fig. 1 Geometry of Gaussian bump in channel. Boundary conditions: subsonic inflow (——), slip wall (——), and subsonic outflow (——).
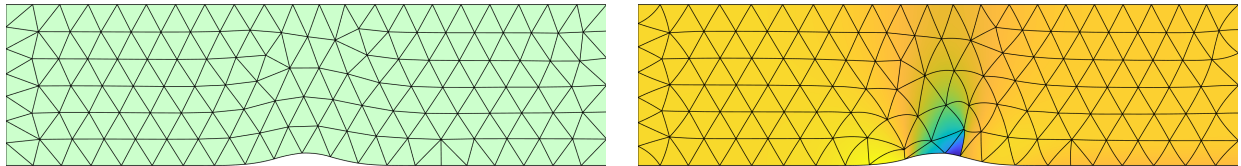
C. Mandatory campaign

All participants will simulate this flow on a sequence of discretizations and report: a succinct description of the discretization, the number of degrees of freedom, the shock attachment point to the wall, and the L_2 stagnation enthalpy error

$$\|H - H_\infty\|_{L_2(\Omega)} = \sqrt{\int_\Omega |H - H_\infty|^2 \, dV}, \tag{2}$$

where $\Omega \subset \mathbb{R}^2$ is the flow domain and $H : \Omega \to \mathbb{R}$ is the pointwise enthalpy from the flow solution.

D. Preliminary results

Preliminary results for this problem were computed using the High-Order Implicit Shock Tracking (HOIST) method [2, 3] using Roe's numerical flux on a sequence of unstructured triangular grids with decreasing element sizes for polynomial degrees $p = 1, 2, 3, 4$. The coarsest grid is initially generated using DistMesh [4] and subsequently all high-order nodes were projected onto the curved boundary (Figure 2). Refined meshes are produced by uniformly refining each triangle into four triangles and projecting all new nodes onto the curved boundary (Table 1). Because HOIST is a shock tracking method, degrees of freedom for both the grid and flow solution are reported.

Fig. 2 Coarsest mesh used for transonic bump (*left*) and the corresponding density field and optimized grid for $p = 2$ HOIST method (*right*).

2

Table 1   Convergence study of HOIST method for transonic bump

ref-lvl	p-order	# cells	# mesh DoF	# solution DoF	L_2 error	shock attachment point
0	1	237	948	2844	1.45e-03	(0.10279225135, 0.04799085075)
1	1	948	3790	11376	3.56e-04	(0.10301295362, 0.04793638605)
2	1	3792	15158	45504	9.43e-05	(0.10285594945, 0.04797513704)
0	2	237	948	5688	3.86e-04	(0.10533751557, 0.04735946775)
1	2	948	3790	22752	4.22e-05	(0.10279591661, 0.04798994669)
2	2	3792	15158	91008	6.45e-06	(0.10285179563, 0.04797616188)
0	3	237	948	9480	3.30e-04	(0.10441521835, 0.04758906991)
1	3	948	3790	37920	2.03e-05	(0.10282109770, 0.04798373520)
0	4	237	948	14220	2.32e-04	(0.10213585482, 0.04815250856)
1	4	948	3790	56880	9.46e-06	(0.10275102462, 0.04800101854)

III. Steady, viscous, transonic flow: Sajben transonic diffuser

The second test problem is viscous flow through the Sajben transonic diffuser. The problem features fully turbulent flow, a normal shock, and shock-induced flow separation. It is intended to assess the ability of CFD methods to handle these features in a relatively simple two-dimensional geometry.

A. Geometry and Meshes

The Sajben diffuser geometry is described by Bogar et al. [5] and reproduced in Figure 3. The profile of the upper wall, for $x \in [-4.04h, 8.65h]$, is

$$y(x) = \begin{cases} 1.4h & -4.04h \leqslant x < \ell_c \\ y_c(x) & \ell_c \leqslant x < 0 \\ y_d(x) & 0 \leqslant x < \ell_d \\ 1.5h & \ell_d < x \leqslant 8.65h, \end{cases} \tag{3}$$

where

$$y_c(x) = \frac{\alpha_c \cosh \zeta_c(x)}{(\alpha_c - 1) + \cosh \zeta_c(x)}, \qquad y_d(x) \frac{\alpha_d \cosh \zeta_d(x)}{(\alpha_d - 1) + \cosh \zeta_d(x)} \tag{4}$$
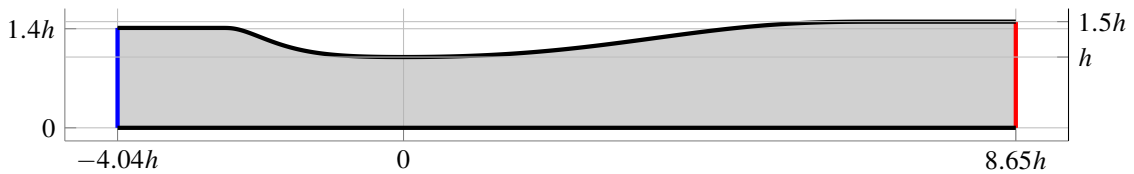
and

$$\zeta_c(x) = \frac{C_1(x/\ell_c)(1 + C_2(x/\ell_c))^{C_3}}{(1 - x/\ell_c)^{C_4}}, \qquad \zeta_d(x) = \frac{D_1(x/\ell)_d}{(1 - x/\ell_d)^{D_4}}, \tag{5}$$

with parameters $\alpha_c = 1.4114$, $\ell_c = -2.598h$s, $C_1 = 0.81$, $C_2 = 1.0$, $C_3 = 0.5$, $C_4 = 0.6$, $\alpha_d = 1.5$, $\ell_d = 7.216h$, $D_1 = 2.25$, $D_4 = 0.6$, and $h = 44$mm

B. Governing equations

The compressible Navier-Stokes equations should be simulated using the perfect gas assumption (e.g. single species, constant specific heat) and Sutherland's Law for viscosity. The flow should be simulated both without a turbulence

Fig. 3   Geometry of Sajben diffuser.   Boundary conditions: subsonic inflow (——), viscous wall (——), and subsonic outflow (——).

Table 2   Flow conditions for Sajben diffuser problem

Specific heat ratio, γ	1.4
Mach Number, M_∞	0.4
Inlet total pressure	19.58 psi
Inlet total temperature	278 K
Outlet static pressure	14.10 psi
Freestream Reynolds Number, Re_∞	7.0×10^5 m^{-1}
Prandtl Number, Pr	0.71

model and with the negative Spalart-Allmaras turbulence model [6]. The flow conditions are shown in Table 2. The inflow and outflow boundaries can use the condition that is most appropriate for the flow solver used. The wall boundary condition is an adiabatic, no-slip condition.

C. Mandatory campaign

All participants will simulate this flow on a sequence of discretizations. For each mesh and turbulence model, participants should report the x-directed force integrated over the top and bottom walls, the flow separation location, and the static pressure profile along the top and bottom walls. Furthermore, a succinct description of the numerical method used should be provided as well as algorithmic details (e.g., how is the flow initialized, if/how is adaptation incorporated). Finally, the nonlinear residual convergence and work units should be reported.

IV. Steady, viscous, hypersonic flow: HIFiRE-1

The purpose of this case is to evaluate the ability of solvers to predict heating on the surface of a relevant geometry at an angle of attack in hypersonic flow. The HIFiRE-1 geometry is a blunt sphere-cone with a cylindrical section and a flare [7].
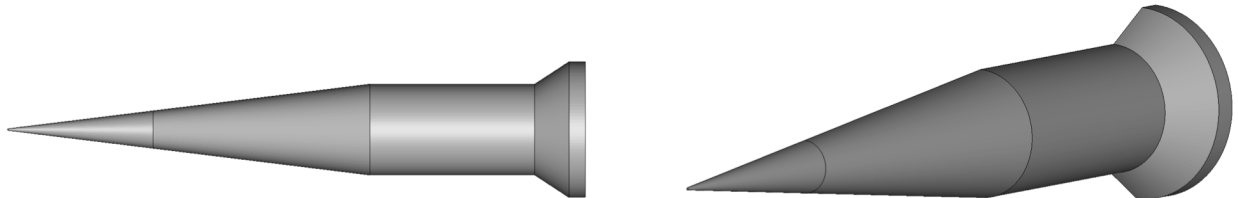
A. Geometry

The HIFiRE-1 geometry is described in [7] and reproduced in Figure 4.

B. Governing equations

The compressible Navier-Stokes equations should be simulated using the perfect gas assumption (e.g. single species, constant specific heat) and Sutherland's Law for viscosity. The flow should be simulated both without a turbulence model and with the negative Spalart-Allmaras turbulence model[6]. The flow conditions are shown in Table 3. The inflow and outflow boundaries can use the condition that is most appropriate for the flow solver used. The wall boundary condition is an isothermal, no-slip condition with a wall temperature ratio given by

$$T_w/T_\infty = 1.279, \tag{6}$$

where T_w is the isothermal wall temperature and T_∞ is the static freestream temperature.

Fig. 4   HIFiRE-1 geometry

Table 3   Flow conditions for HIFiRE-1 problem

Specific heat ratio, γ	1.4
Mach Number, M_∞	7.18
Freestream Reynolds Number, Re_∞	10.123×10^6 m^{-1}
Prandtl Number, Pr	0.72
Angle of attack, α	$2°$
Wall temperature ratio, T_w/T_∞	1.279

C. Mandatory campaign

All participants will simulate this flow on a sequence of discretizations. For each mesh and turbulence model, participants should report wall heat flux and pressure profiles. These profiles should be: (a) along the intersection of the wall and the y-z plane on the windward side, (b) along the intersection of the wall and the y-z plane on the lee side, and (c) along the intersection of the wall and the x-z plane. Pressure should be non-dimensionalized by p_∞ and heat flux should be non-dimensionalized by $\kappa_\infty T_\infty/r$, where κ_∞ is the freestream thermal conductivity and $r = 0.137275$m is the radius of the cylindrical section. Furthermore, a succinct description of the numerical method used should be provided as well as algorithmic details (e.g., how is the flow initialized, if/how is adaptation incorporated). Finally, the nonlinear residual convergence and work units should be reported.

V. Unsteady, inviscid, supersonic flow: shock-vortex interaction

This case was designed to demonstrate a solver's ability to capture the complex flow phenomena that result from the interaction of a traversing vortex and a standing shock wave. This case was part of the AIAA High Fidelity CFD Workshop 2022 and the predecessor 5th International Workshop on High-Order CFD Methods. It is a two-dimensional, unsteady, inviscid problem. Two flow features are prominent in results from this case: the initial vortex is split into two distinct vortical structures after passing through the shock, and cylindrical acoustic waves appear downstream of the stationary shock, centered on the moving vortex. Density contours from example results are shown in Figure 5.

A. Geometry and Meshes

The geometry of the domain is shown in Figure 6. The top and bottom boundaries are slip walls, and the left and right boundaries are a supersonic source and a subsonic sink, respectively. Meshes will consist of either regular quadrilateral elements or irregular mixed elements. The names for each mesh will start with RQ for the regular quadrilateral elements and IM for the irregular mixed elements, and they will end with the reciprocal of the element length scale, e. g., a regular quadrilateral mesh with elements sized 0.02 units is named RQ50. Q1 CGNS meshes will be provided for RQ50, RQ100, RQ150, RQ200, RQ250, RQ300, RQ400, and RQ500. GMSH scripts will be provided to create IM meshes as well as any additional RQ meshes.

B. Governing equations

The two-dimensional Euler equations are employed for a perfect gas with the ratio of specific heats, $\gamma = 1.4$, and unit non-dimensionalized gas constant, $R = 1$. The flow is initialized with a standing shock at location $x = 0.5$ with a strength given by the upstream Mach number, $M_u = 1.5$, and a vortex centered at $(0.25, 0.5)$ with $M_v = 0.9$. The upstream flow quantities are $(\rho, u, v, p) = (1.0, 1.775, 0.0, 1.0)$, outside of the vortex. The downstream properties are computed using normal shock relations. The vortex angular velocity is given by

$$v_\theta = \begin{cases} v_m \frac{r}{a} & r \leqslant a \\ v_m \frac{a}{a^2 - b^2} \left(r - \frac{b^2}{r} \right) & a < r \leqslant b \\ 0 & r > b \end{cases},$$

where r is the radial distance from the vortex center, $(a, b) = (0.075, 0.175)$ define the inner and outer regions of the vortex, and $v_m = M_v \sqrt{\gamma}$ is the maximum angular velocity. The following ODE is used to compute the temperature as a
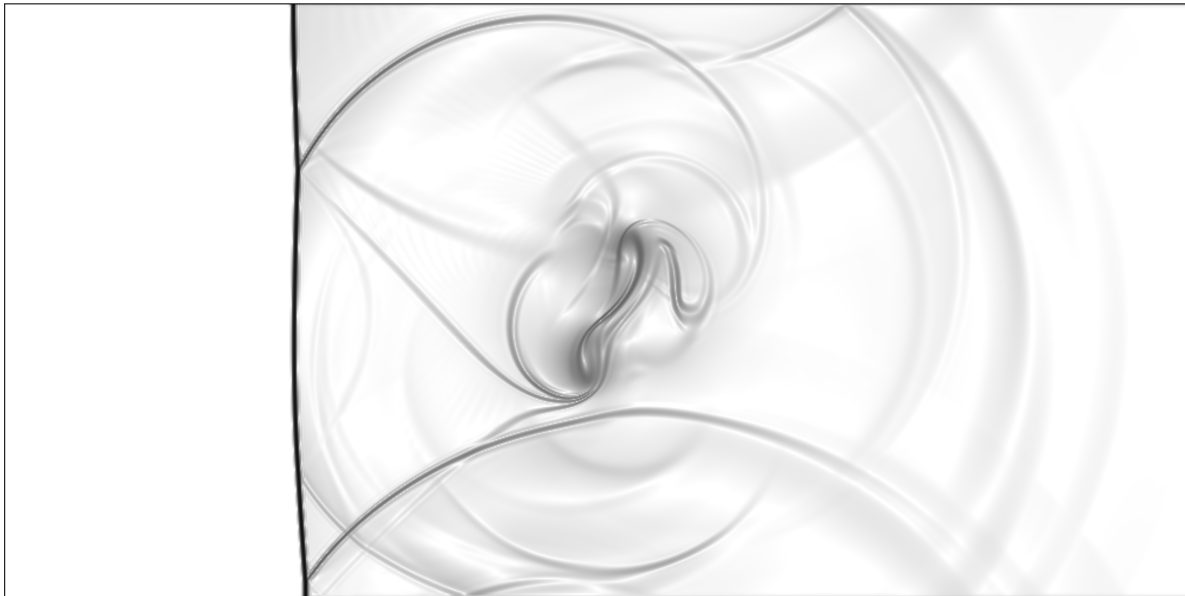
Fig. 5   Example results showing Schlieren contours at time $t = 0.7$. [8]
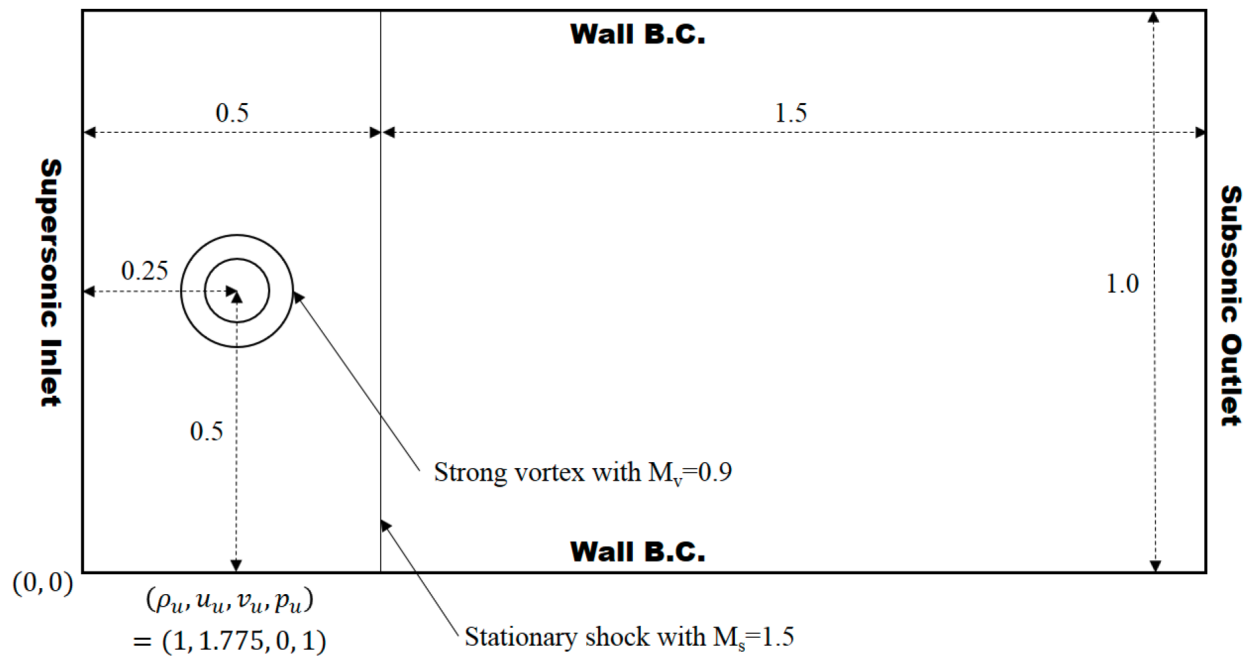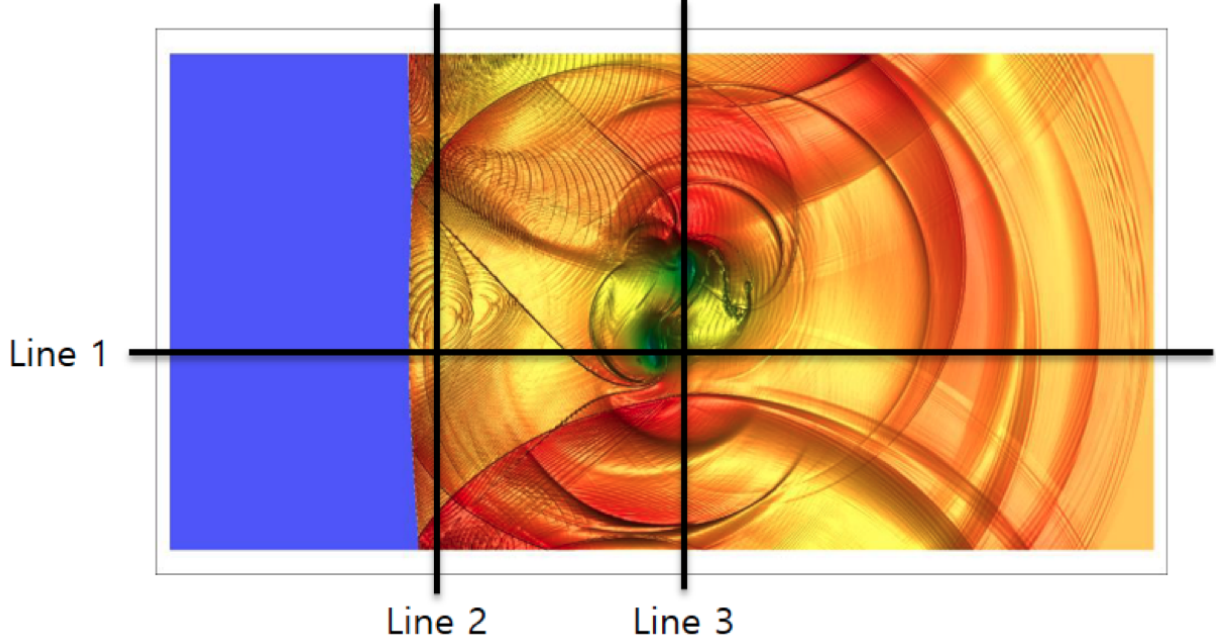

Fig. 6   Geometry for the shock-vortex interaction. Image taken from AIAA High Fidelity CFD Workshop 2022 case description.

6

Fig. 7 **Data extraction lines for the shock-vortex interaction. Image taken from AIAA High Fidelity CFD Workshop 2022 case description.**

function of radial distance, where R is the gas constant,

$$\frac{dT(r)}{dr} = \frac{\gamma - 1}{R\gamma} \frac{v_\theta(r)^2}{r}.$$

Isentropic relations are used to compute the pressure field. A python script will be provided to aid in setting up the initial conditions.

C. Mandatory campaign

All participants will simulate this flow on a sequence of spatial and temporal discretizations. Participants will provide a brief summary of their numerical method used as well as algorithmic details. For each spatial and temporal discretization level, participants will provide the integrated total enthalpy over the domain at time $t = 0.7$ along with the data items listed below.

Participants will provide density along three lines, shown in Figure 7, at time $t = 0.7$. The lines are specified along $y = 0.4$, $x = 0.52$, and $x = 1.05$, and they provide, respectively, a longitudinal view through the standing shock wave and adjacent to the primary vortex core, a transverse view parallel to and just downstream of the standing shock wave, and a transverse view through the primary vortex core. The points along each line are specified as follows:

- Line 1: $P_i = (x_i, \alpha + \epsilon)$, where $x_i = \frac{h}{2} + (i - 1) \times h, h = \frac{2}{N}, i = 1, ..., N$
- Line 2,3: $P_i = (\beta + \epsilon, y_i)$, where $y_i = \frac{h}{2} + (i - 1) \times h, h = \frac{1}{N}, i = 1, ..., N$
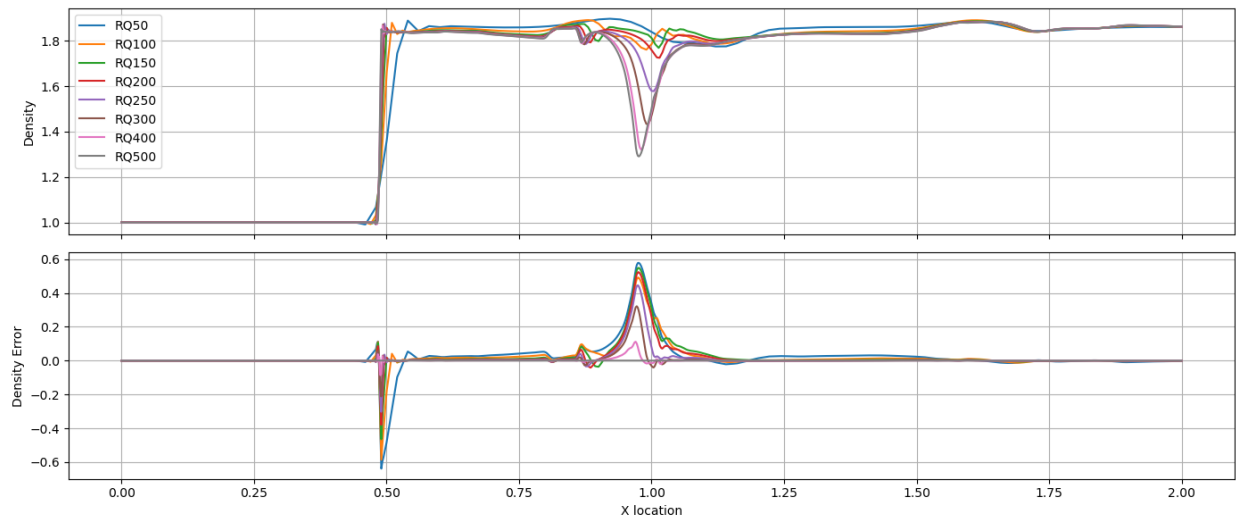
where $\epsilon = 0.0001$ is added to avoid overlap with cell interfaces. The α/β and N values for each line are:

- Line 1: $(\alpha, N) = (0.4, 8000)$
- Line 2: $(\beta, N) = (0.52, 4000)$
- Line 3: $(\beta, N) = (1.05, 4000)$

Participants will also provide two contour images of the Schlieren variable at time $t = 0.7$. This value is defined by

$$Sch = \log_{10}(1 + ||\nabla\rho||).$$

Both images will be grayscale and span contour values from 0.05 to 2.4, inclusive. The first image will cover the entire domain $x \in [0, 2]$ and $y \in [0, 1]$, and the second image will only contain the vortex in the subdomain $x \in [0.9, 1.2]$ and $y \in [0.33, 0.63]$.

7

Fig. 8   Sample density and density error results along line 1 at $y = 0.4$ **on each Q1 mesh with SDIRK45 4th-order time integration and time step 0.001 at time** $t = 0.7$**. [8]**
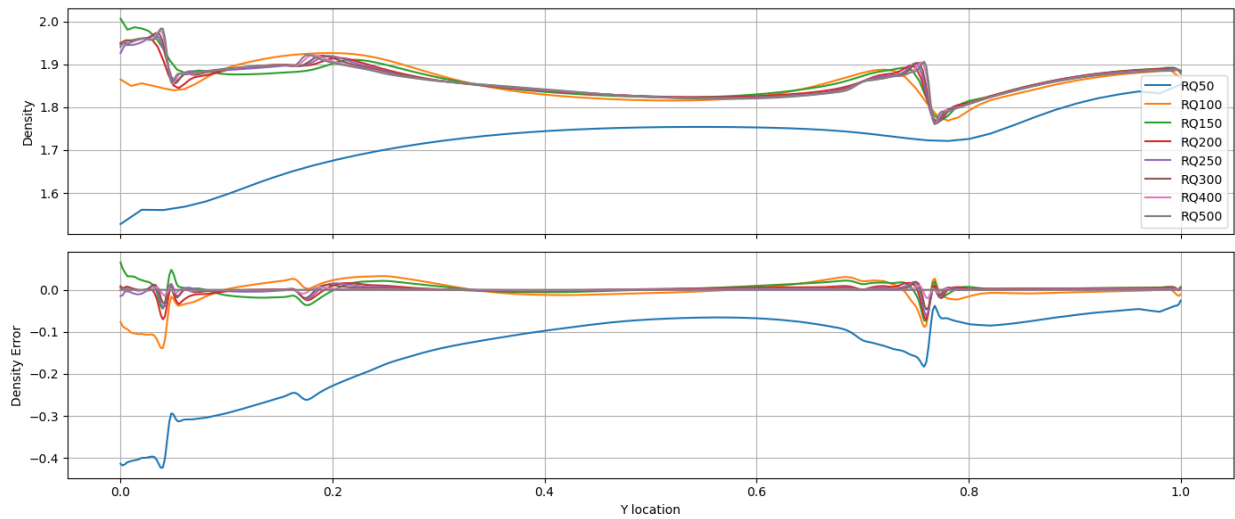
D. Preliminary results

Preliminary results are provided from simulations run using the COFFE solver within Kestrel. These results were originally reported by Holst et al. [8] at the AIAA 2022 Scitech Forum, and more information about the solver and case set up can be found in the paper.
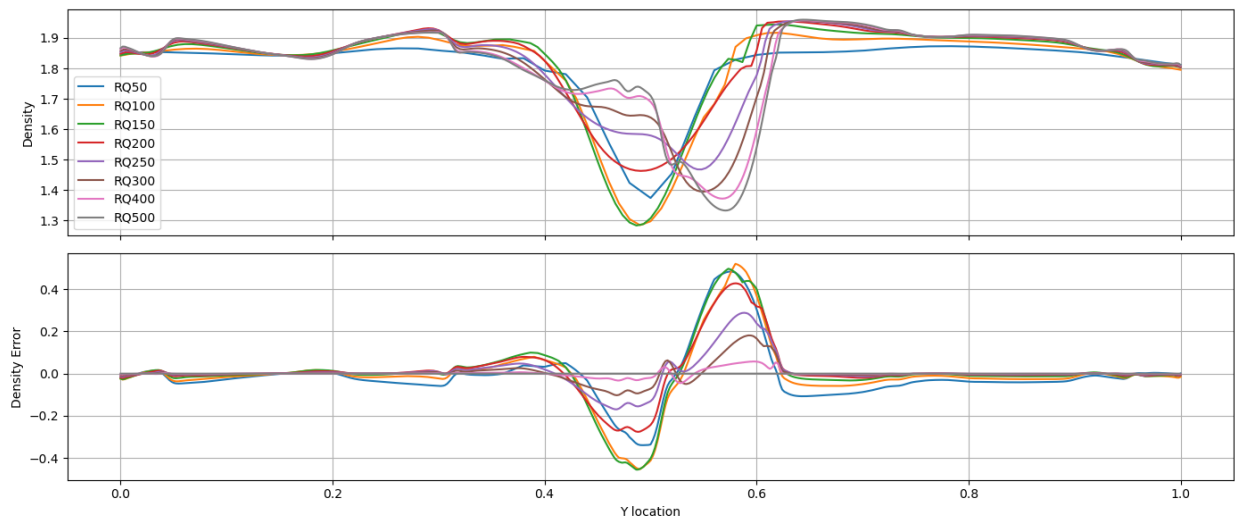
Density and density error along lines 1, 2, and 3 are shown in Figures 8 to 10 for each of the Q1 RQ meshes. All cases were run with a time step of $\Delta t = 0.001$ and using a 4th-order, 5-stage, singly diagonally implicit Runge-Kutta method (SDIRK45) for time integration. The plots, particularly Figure 10, depict the final flowfield's dependence on the spatial resolution.

Plots of Schlieren contours for each mesh size with the SDIRK45 time integration scheme and time step $\Delta t = 0.001$ at time $t = 0.7$ are shown in Figure 11. The final flowfield's dependence on spatial resolution is also depicted in these figures. The coarsest mesh introduces a large amount of dissipation error, which results in an overly diffuse flowfield where only the strongest features are present. Dissipation error is reduced with mesh refinement, allowing weaker flow structures to become visible. [8]
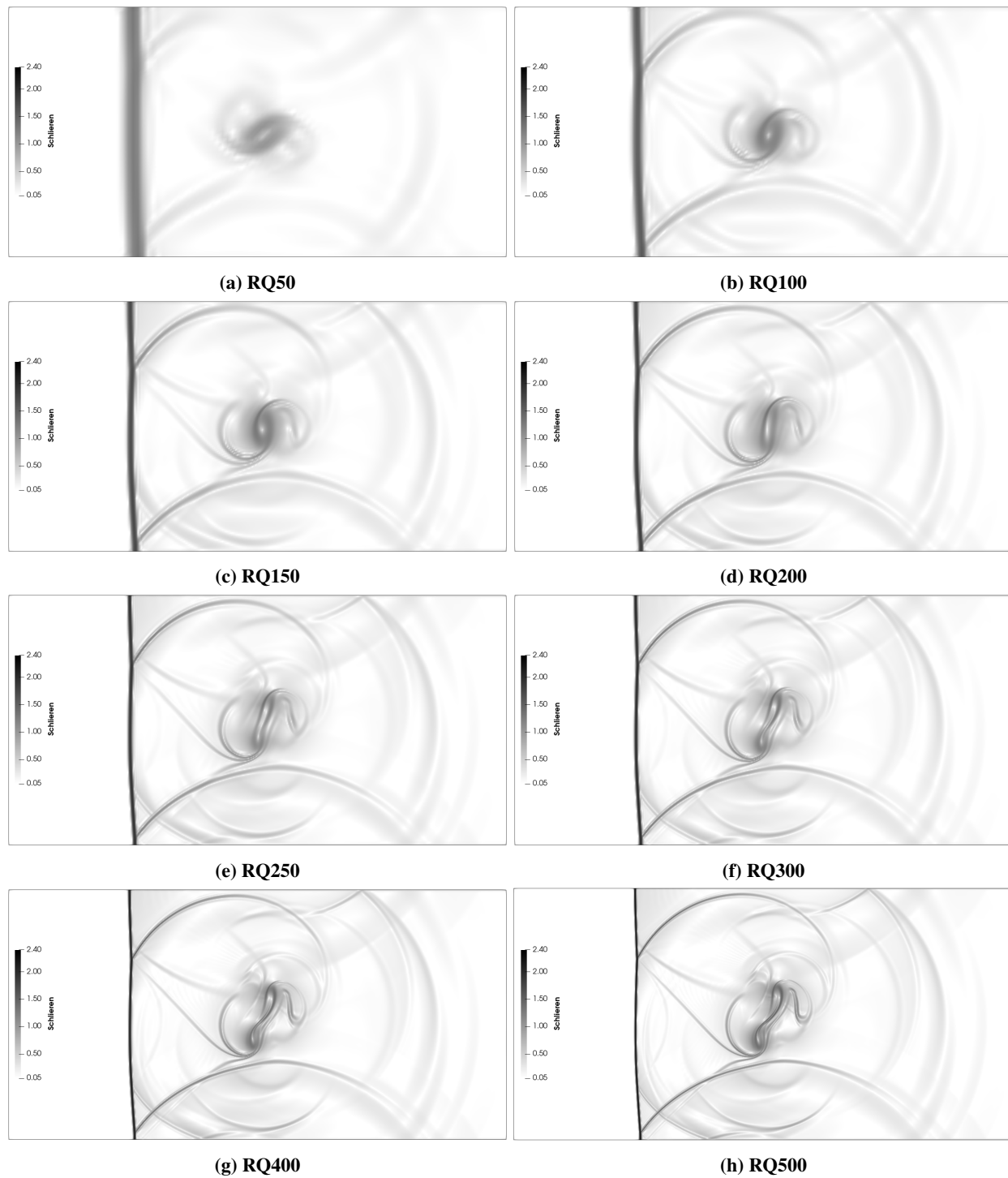
Fig. 9 Sample density and density error results along line 2 at $x = 0.52$ on each Q1 mesh with SDIRK45 4$^{\text{th}}$-order time integration and time step 0.001 at time $t = 0.7$. [8]

Fig. 10 Sample density and density error results along line 3 at $x = 1.05$ on each Q1 mesh with SDIRK45 4$^{\text{th}}$-order time integration and time step 0.001 at time $t = 0.7$. [8]

(a) RQ50

(b) RQ100

(c) RQ150

(d) RQ200

(e) RQ250

(f) RQ300

(g) RQ400

(h) RQ500

Fig. 11 Sample Schlieren contours on each Q1 mesh with SDIRK45 4th-order time integration and time step 0.001 at time $t = 0.7$**. [8]**

Acknowledgments

References

[1] Wang, Z. J., Fidkowski, K., Abgrall, R., Bassi, F., Caraeni, D., Cary, A., Deconinck, H., Hartmann, R., Hillewaert, K., Huynh, H. T., et al., "High-order CFD methods: current status and perspective," *International Journal for Numerical Methods in Fluids*, Vol. 72, No. 8, 2013, pp. 811–845.

[2] Zahr, M. J., Shi, A., and Persson, P.-O., "Implicit shock tracking using an optimization-based high-order discontinuous Galerkin method," *Journal of Computational Physics*, Vol. 410, 2020, p. 109385. doi: https://doi.org/10.1016/j.jcp.2020.109385.

[3] Huang, T., and Zahr, M. J., "A robust, high-order implicit shock tracking method for simulation of complex, high-speed flows," *Journal of Computational Physics*, Vol. 454, 2022, p. 110981. doi: https://doi.org/10.1016/j.jcp.2020.109385.

[4] Persson, P.-O., and Strang, G., "A simple mesh generator in MATLAB," *SIAM Review*, Vol. 46, No. 2, 2004, pp. 329–345.

[5] Bogar, T. J., Sajben, M., and Kroutil, J. C., "Characteristic frequencies of transonic diffuser flow oscillations," *AIAA Journal*, Vol. 21, No. 9, 1983, pp. 1232–1240. doi: 10.2514/3.8234.

[6] Allmaras, S., and Johnson, F., "Modifications and clarifications for the implementation of the Spalart-Allmaras turbulence model," *Seventh International Conference on Computational Fluid Dynamics (ICCFD7)*, Vol. 1902, 2012.

[7] Wadhams, T., Mundy, E., MacLean, M., and Holden, M., "Ground test studies of the HIFiRE-1 transition experiment part 1: experimental results," *Journal of Spacecraft and Rockets*, Vol. 45, No. 6, 2008, pp. 1134–1148.

[8] Holst, K. R., Glasby, R. S., and Erwin, J. T., "Current Status of the Finite-Element Fluid Solver (COFFE) within HPCMP CREATE TM -AV Kestrel," *AIAA Scitech 2022 Forum*, 2022. doi: 10.2514/6.2022-0024.